Multiple-scattering $X\alpha$ study of the silicon and chlorine core-level photoabsorption spectra of $SiCl_4$

J. S. Tse*
Division of Chemistry, National Research Council of Canada, Ottawa, Ontario, Canada K1A 0R9

Z. F. Liu, J. D. Bozek, and G. M. Bancroft
Department of Chemistry and Center for Chemical Physics, University of Western Ontario, London, Ontario, Canada N6A 5B7 and Canadian Synchrotron Radiation Facility, Synchrotron Radiation Center, University of Wisconsin, Stoughton, Wisconsin 53589
(Received 22 August 1988)

The Si 1*s*, 2*s*, 2*p*, and Cl 1*s*, 2*p* photoabsorption spectra of $SiCl_4$ have been assigned with the aid of multiple-scattering $X\alpha$ calculations. The strongest pre-edge absorptions are assigned to transitions to Si—Cl antibonding orbitals. The weaker complex features observed near the ionization threshold can be ascribed to electronic excitations into Rydberg orbitals. The calculations also show that the weak structures beyond the Si absorption edge are mainly due to resonances in the e^* and t_2^* continuum channels. Eigenphase sums indicate that the high-energy (≥ 20 eV) above-edge resonances are due to photoelectron diffraction.

INTRODUCTION

Recent advances in electron-energy-loss spectroscopy[1] and the availability of dedicated synchrotron radiation sources[2] have stimulated much recent interest in the study of core-level absorption spectra of gaseous inorganic polyatomic molecules.[3] Recent high-resolution 2*p* spectra (≤ 0.1 eV photon width) of Si compounds[4-6] emphasize the complexity of such spectra, and the enormous theoretical challenge to interpret both pre-edge and post-edge regions. Although two recent studies[5,6] have addressed the discrete pre-edge region of SO_2 and PX_3 compounds in detail, most studies have concentrated on the post-edge or near-edge x-ray-absorption fine-structure (NEXAFS) region where so-called *shape*[7] or *giant*[8] resonances are observed. Excellent reviews on this subject have been published recently.[9] The phenomenon of *shape* resonances was first observed in the core-level spectra of highly fluorinated molecules.[7,10] The sudden enhancement in absorption was attributed to electronic excitation into quasibound unoccupied orbitals supported by a potential barrier created by the electronegative ligands.[7] An alternative explanation has been proposed which shows that interactions of antibonding orbitals with the bound Rydberg and/or continuum orbitals causes the above-edge resonances.[8,11,12] Very recent studies show that resonant enhancement in photoabsorption and photoionization cross sections can occur in molecules without electronegative ligands,[13,14] or antibonding orbitals in the continuum,[15] and that atomic scattering of the photoelectron is important for producing many post-edge features.[16]

As part of an extended study of the core-level edges in silicon compounds, we report, in this article, the results of a theoretical multiple-scattering (MS) $X\alpha$ study of the Si 2*p*, Si 2*s*, Si 1*s*, and Cl 2*p* spectra of $SiCl_4$. High-resolution spectra of these edges have been previously reported recently.[4,17] Although the post-edge *shape* resonance features of the Si 2*p* and Si 2*s* edges have been assigned with the aid of MS $X\alpha$ calculations, the pre-edge spectra of all four levels and the above-edge Si 1*s* spectrum are not well understood. The features observed in the 1*s* (Ref. 17) and 2*s* (Ref. 4) spectra are similar. The strong pre-edge peak 4.7 eV below the edge can be readily assigned to a symmetry-allowed excitation from the 1*s* or 2*s* level to a Si-Cl t_2^* antibonding level, but the assignment of the broadband near threshold is puzzling.[17] In a previous study of the Si 1*s* photoabsorption spectrum,[17] it was argued that excitation to Rydberg levels would not be important due to the large chlorine ligands masking any contribution to *outer well* Rydberg states. The band was tentatively assigned to a symmetry-forbidden transition to the antibonding a_1^* orbital. The pre-edge Si 2*p* spectrum is even more puzzling.[4,19,20] Six spin-orbit-split pairs of transitions were identified in the high-resolution spectrum. Although two pairs of transitions may be assigned to excitations into the antibonding t_2^* and a_1^* orbitals, the assignment of the remainder of the spectrum is difficult.

The standard MS $X\alpha$ method[21,22] was used to calculate the bound-transition oscillator strengths[23] and the continuum MS $X\alpha$ method[24,25] was used to calculate the ionization cross sections. The MS $X\alpha$ method has been demonstrated to be an efficient and reliable method for generating Rydberg[26-28] and continuum orbitals.[29] The excitation energies, calculated with the transition-state procedure,[30] are often within a few eV of the observed values. In most cases, the calculated oscillator strengths of the bound-state transitions[23] and the photoionization cross sections[31] are also in semiquantitative agreement with experiment. Therefore, the theoretical results obtained from MS $X\alpha$ calculations can be very useful in guiding the assignments of core-level photoabsorption spectra.

COMPUTATIONAL DETAILS

The above-edge region of the Si $2p$ ionization cross section of $SiCl_4$ has been studied using the MS $X\alpha$ method previously,[18,32] and the same set of parameters was adopted here. In essence, the internuclear Si-Cl distance was taken as 3.800 a.u. Overlapping atomic-sphere radii were taken to be 2.150 a.u. for Si and 2.000 a.u. for the Cl. The partial-wave expansions (l_{max}) were terminated at 4 for the outer sphere and at 2 for the Si and Cl spheres. In the continuum calculations, the l_{max} were expanded to 7 and 3 for the outer and atomic spheres, respectively. A constant-exchange parameter of 0.72 was used in all regions of the calculation. A Latter tail[3] was added to the outer-sphere potential during the self-consistent iteration to account for the asymptotic behavior of the potential at large distances. Following previous work,[18,32] the photoionization cross sections were calculated using a transition-state potential with half of an electron removed from the outermost valence orbital. The core-level excitation energies and oscillator strengths were calculated with the appropriate transition-state potentials. The calculated valence orbital[32] and Si $2p$ (Ref. 18) photoionization cross sections are identical to those reported previously.

In the calculations of the Cl $2p$ edge, a localized core-hole scheme was adopted. Thus the symmetry of the $SiCl_4$ molecule was lowered from T_d to C_{3v}. In a previous study of carbon core-level shakeup in group-IIB metal dimethyl compounds,[34] we found that the localized core-hole approximation[35,36] gave very reasonable transition energies and intensities.

RESULTS AND DISCUSSION

Pre-edge region

The charge distributions of the unoccupied orbitals found by an energy search up to -0.1 Ry, with the Si $1s$ transition-state potential are summarized in Table I. The electronic charge of the two lowest-energy orbitals, $8a_1^*$ and $9t_2^*$, is concentrated in the atomic and intersphere regions. Inspection of the relevant wave functions [Figs. 1(a) and 1(b)] shows substantial antibonding character along the Si—Cl bonds. Incidentally, the calculated order of the unoccupied orbitals is similar to that in SiF_4 in which the two lowest empty orbitals are known to be antibonding a_1^* and t_2^*.[37] The higher-energy $9a_1^*$, $10t_2^*$, $11t_2^*$, $3e^*$, and $10a_1^*$ orbitals are more diffuse (Fig. 2) with most of the electron density residing in the outer-sphere region. These orbitals may be classified as conjugate Rydberg or Rydberg orbitals.[38–40]

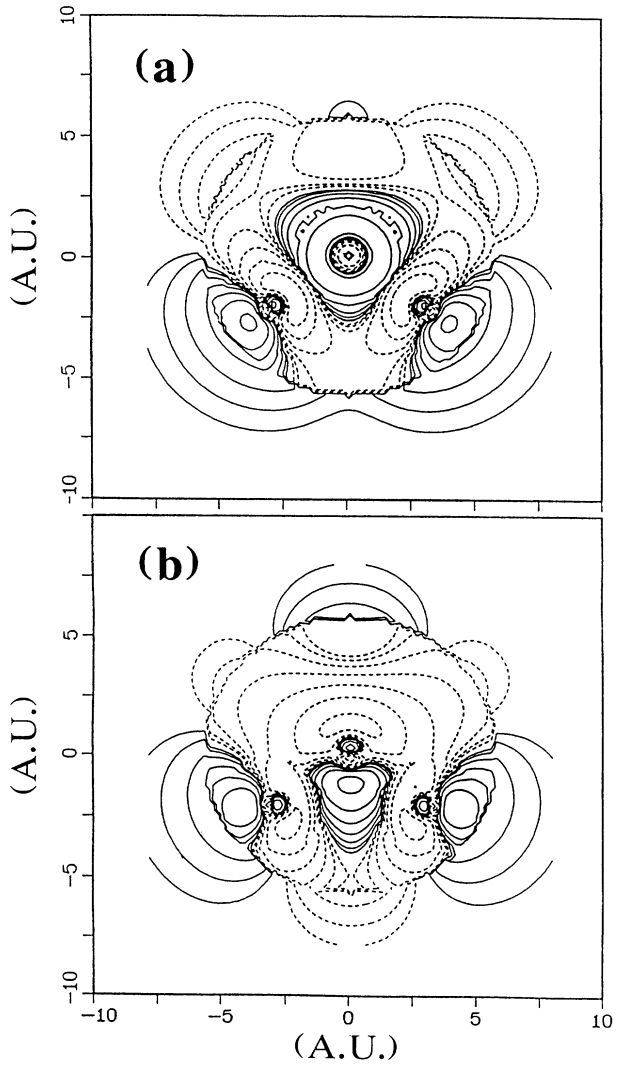

FIG. 1. Contour diagrams for the Si—Cl antibonding wave functions (a) $8a_1^*$ and (b) $9t_2^*$, plotted in a plane containing the Si and two Cl ligands.

Considering the Si $1s$ and Si $2s$ regions first, the only symmetry-allowed excitations from the s core levels are

TABLE I. Orbital charge distribution for the unoccupied orbitals in the Si $2p$ core transition state of $SiCl_4$.

Orbital	Q_{out}	Q_{int}	Q_{Si}	Q_{Cl}	Remarks
$8a_1^*$	0.05	0.19	0.23	0.53	Si—Cl antibonding
$9t_2^*$	0.04	0.30	0.35	0.31	Si—Cl antibonding
$9a_1^*$	0.44	0.50	0.00	0.06	Rydberg s
$10t_2^*$	0.49	0.38	0.04	0.08	Rydberg p
$11t_2^*$	0.68	0.27	0.01	0.04	Rydberg p and d
$3e^*$	0.81	0.14	0.00	0.05	Rydberg d
$10a_1^*$	0.92	0.07	0.00	0.01	Rydberg s

into empty orbitals of t_2 symmetry. Three transitions are predicted by the MS $X\alpha$ calculations: Si $2s$ to the $9t_2^*$ antibonding orbital and the Rydberg $10t_2^*$ and $11t_2^*$ orbitals. The calculated pre-edge spectrum [Fig. 3(a), Table II], after having convoluted with a Lorentzian line shape of half width 0.4 eV, is in good semiquantitative agreement with the experimental spectrum,[4] which shows an intense peak at 4.7 eV below the edge and a weaker peak at 1.0 eV and we can readily assign the first peak to Si $2s \rightarrow 9t_2^*$ and the second peak mainly to Si $2s \rightarrow 10t_2^*$. The excitation to the Rydberg $10t_2^*$ and $11t_2^*$ orbitals resembles atomic $s \rightarrow p$ transitions, and somewhat surprisingly the Si $2s \rightarrow 10t_2^*$ transition has about 20% of the intensity of the Si $2s \rightarrow 9t_2^*$ transition. The calculated intensity ratio $9t_2^*$: $10t_2^*$ of ~ 6 is in good agreement with the experimental ratio of ~ 5, and the calculated and observed peak positions (after correcting for the energy required to match the experimental I.P.) are also in reasonable agreement. The calculated separation of the two peaks of 2.0 eV compares with the observed splitting of

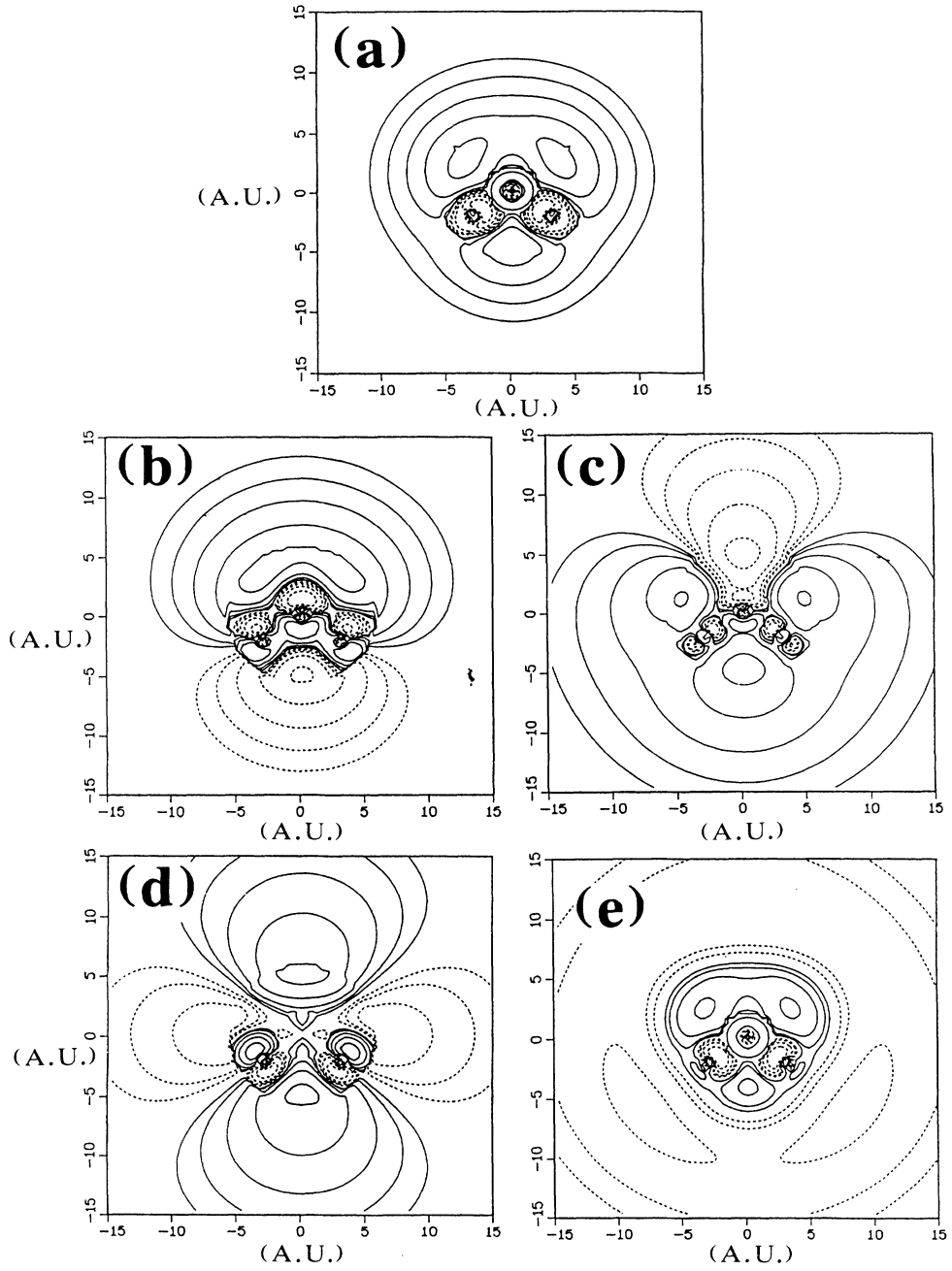

FIG. 2. Contour diagrams for the Rydberg wave functions (a) $9a_1^*$, (b) $10t_2^*$, (c) $11t_2^*$, (d) $3e^*$, and (e) $10a_1^*$.

3.7 eV.[4]

The profile of the Si 1s (Ref. 12) photoabsorption spectrum closely resembles the Si 2s spectrum. The main feature in the Si 1s spectrum is a strong peak at 4.7 eV below threshold followed by a broad and weaker band very near the ionization edge. The intensity ratio of the first to the second peak is again very close to 6. The theoretical spectrum [Fig. 3(b)] is again very similar to the Si 2s theoretical spectrum (after including a broader linewidth of 0.8 eV for the larger photon width and inherent linewidth). The Si 1s spectrum can then be assigned in an identical way to the Si 2s spectrum: the large first peak is due to the Si $1s \rightarrow 9t_2^*$ excitation, while the weaker second peak is assigned to the Si $1s \rightarrow 10t_2^*$ excitation. The assignment of the first peak agrees with those proposed earlier. However, the assignment of the second peak to Rydberg transitions is at variance with a previous assignment. In the earlier work,[17] it was argued that the potential barrier created by the electronegative chlorine ligands would restrict the diffuse Rydberg orbitals to the *outer well* region and, consequently, the overlap of these orbitals with the core orbital would be small. The second peak was then assigned to a formally forbidden $1s \rightarrow 8a_1^*$ transition which became allowed when the excited molecule distorted from T_d symmetry. This explanation, however, is not convincing. As shown in the contour diagrams (Fig. 1), low-angular-momentum Rydberg wave functions can penetrate into the *inner-well* region and acquire some valence character. Small, but significant oscillator strengths result for excitations into these Rydberg orbitals.

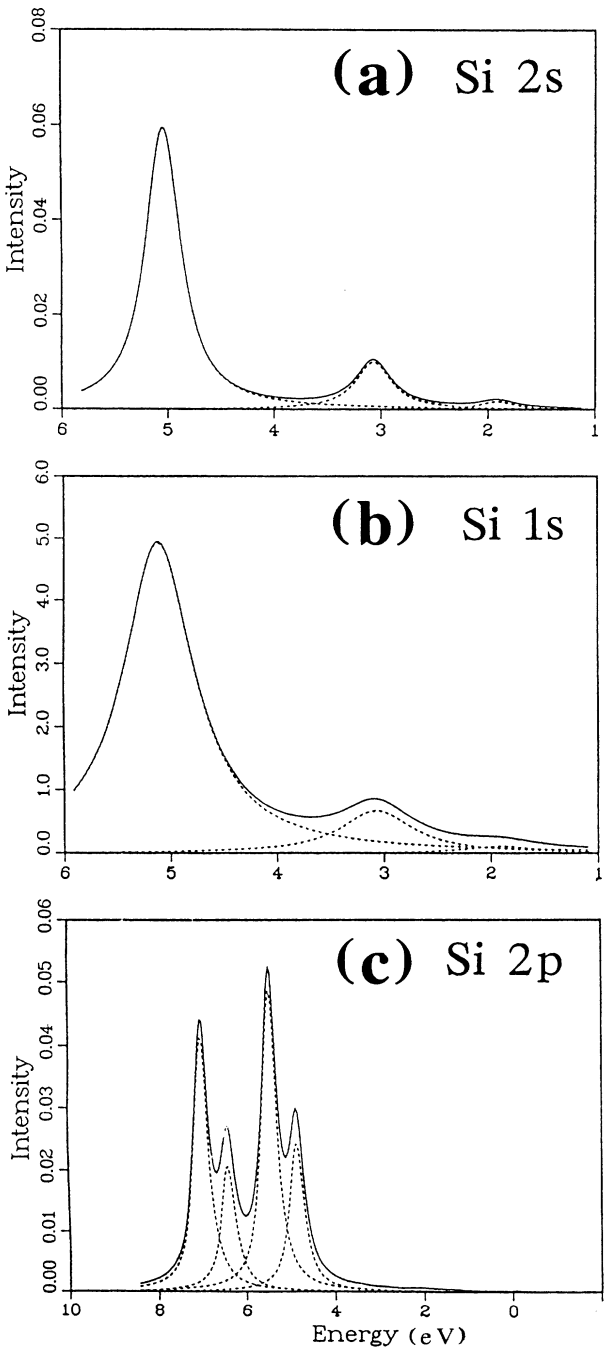

FIG. 3. Pre-edge of (a) Si 2s, (b) Si 1s and (c) Si 2p.

The extremely similar experimental and theoretical Si 2s and Si 1s spectra show once again that the term values of unoccupied orbitals derived from different core levels do not vary significantly, provided that the shielding-antishielding effects of the core holes are comparable.[8,27,39] The orbital energies of corresponding unoccupied orbitals obtained from the Si 1s, 2s, and 2p transition-state potentials show a maximum difference of less than 0.5 eV. Moreover, the character of the corresponding unoccupied orbitals (Table I) does not change significantly with the exact nature of the potential

The Si 2p photoabsorption spectrum is inherently more complex than the Si s core-level spectra. The Si 2p orbitals of $SiCl_4$ transform as triply degenerate t_2 in T_d symmetry and, according to the dipole selection rule, excitations into empty orbitals of a_1, e, t_1, and t_2 symmetry are all allowed. The high-resolution Si 2p spectrum was previously assigned with six spin-orbit pairs in the pre-edge region.[4] All the peaks are very narrow. The three lowest-energy peaks (1–3) and the highest-energy peak (6) are all intense, while the fourth and fifth peaks are much weaker. Interestingly, the intensities of the spin-orbit pairs derived from the Si $2p_{3/2}$ and Si $2p_{1/2}$ all deviate greatly from the expected statistical ratio of 2:1. A future paper on the Me_nSiCl_{4-n} compounds will suggest an assignment of seven spin-orbit doublets to better fit the spectrum.

Comparison of the term values (Table II) with those in the Si s core-level spectra (Table II) strongly suggests that the second peak(s) be assigned to Si $2p \rightarrow 9t_2^*$. The first peak is readily assigned to the Si 2p excitation to the antibonding $8a_1^*$ orbital in view of the intensity of the peak and the fact that it should be at lower energy than the Si $2p \rightarrow 9t_2^*$ peak.

The results of the MS $X\alpha$ calculations on the Si 2p bound excitations are tabulated in Table II. The Si $2p \rightarrow 8a_1^*$ transition is predicted to be 1.5 eV lower energy than the Si $2p \rightarrow 9t_2^*$ transition, and is in good accord with the experimental separation between the first and

TABLE II. Experimental and calculated pre-edge structures for $SiCl_4$.

Level	Experimental[a] term value (eV)	Calculated[b] term value (eV)	Oscillator strength	Assignment
Si 2*s*	4.7	5.04	3.74×10^{-2}	$9t_2^*$, Si—Cl antibonding
	1.0	3.07	6.29×10^{-3}	$10t_2^*$, Rydberg *p*
		1.91	9.83×10^{-4}	$11t_2^*$, Rydberg *p,d*
Si 1*s*	4.7	5.11	6.19×10^{-5}	$9t_2^*$, Si—Cl antibonding
	−0.3	3.07	8.37×10^{-6}	$10t_2^*$, Rydberg *p*
		1.90	1.32×10^{-6}	$11t_2^*$, Rydberg *p,d*
Si 2*p*	5.92	6.59	2.60×10^{-2}	$8a_1^*$ Si—Cl antibonding
	4.67	5.05	3.06×10^{-2}	$9t_2^*$, Si—Cl antibonding
	4.25	4.25	1.14×10^{-4}	$9a_1^*$, Rydberg *s*
	2.98	3.08	1.07×10^{-4}	$10t_2^*$, Rydberg *p*
		1.91	5.49×10^{-5}	$11t_2^*$, Rydberg *p,d*
	1.58	1.65	1.16×10^{-4}	$3e^*$, Rydberg *d*
	0.28	1.48	2.89×10^{-5}	$10a_1^*$, Rydberg *s*

[a]Weighed average of $2p_{3/2}$ and $2p_{1/2}$ for Si 2*p* level.
[b]The calculated ionization potentials using transition-state procedure for Si 2*p*, 2*s*, and 1*s* are 113.7, 155.3, and 1855.8 eV, respectively.

second peaks of 1.3 eV. The calculated oscillator strengths show that both transitions will be strong, but the intensities do not match the experiment. Experimentally,[4] the intensity of the first peak(s) is almost double that of the second, while the theoretical oscillator strength for Si $2p\rightarrow8a_1^*$ (2.60×10^{-2}) is smaller than that for the Si $2p\rightarrow9t_2^*$ (3.06×10^{-2}). As expected, the excitations to the higher-energy Rydberg orbitals have much smaller oscillator strengths, but these calculated oscillator strengths are much too small to match the experiment, and the assignment is not readily made. It is surprising that the higher-energy transitions still carry fairly strong intensities in the experimental spectrum.[4] However, considering that the term values for the Si 2*p* transitions should be similar to those for the Si 2*s* and 1*s* transitions, and that there is a t_2^* orbital near threshold from the above-edge calculations,[18] we assign the strong sixth peak(s) near threshold to Si $2p\rightarrow10t_2^*$ and $11t_2^*$ transitions. The much weaker peaks 4 and 5 are not readily assigned by our calculations, although they could be due to other Rydberg transitions such as Si $2p\rightarrow3e^*$ or Si $2p\rightarrow10a_1^*$. There are several possible explanations for the discrepancy in the calculated oscillator strengths and the experimental intensities for the higher excited states. The final state for the excitations from Si 2*p* may be orbitally degenerated. The excited molecule may distort, and transitions formally forbidden in T_d symmetry become allowed.[41,42] The MS $X\alpha$ method is one-electron model, and no configuration mixing of electronic states is taken into account. The neglect of configuration interactions (CI) may affect the distribution of oscillator strengths. This effect is expected to be more important for the weak Rydberg transitions than for the strong bonding-antibonding transitions. More elaborate extended basis-set CI calculations would be useful in providing quantitative comparison with experiment.[43]

Finally, in the pre-edge region, we address the Cl 2*p* and the recently reported Cl 1*s* (Ref. 44) photoabsorption spectra. The Cl 1*s* spectrum is similar to the Si *s* spectra in that it exhibits a relatively simple structure. The experimental spectrum consists of two strong transitions at ~5.5 and ~3.5 eV below the ionization edge, and another weak transition near the threshold. Assuming that the Cl 1*s* core hole is localized on the Cl atom, the relevant symmetry for the excited molecule is C_{3v}. Under transformation from T_d to C_{3v} symmetry, t_2 molecular orbitals split into *e* and a_1 components. The doublet structure of the intense pre-edge transition in the Cl 1*s* spectrum is hence assigned as transitions into the e^* and a_1^* orbitals corresponding to the $9t_2^*$ orbital in the Si *s* spectra. The weaker peak near the threshold also exhibits splitting in the experimental spectrum, but the peaks are very weak.

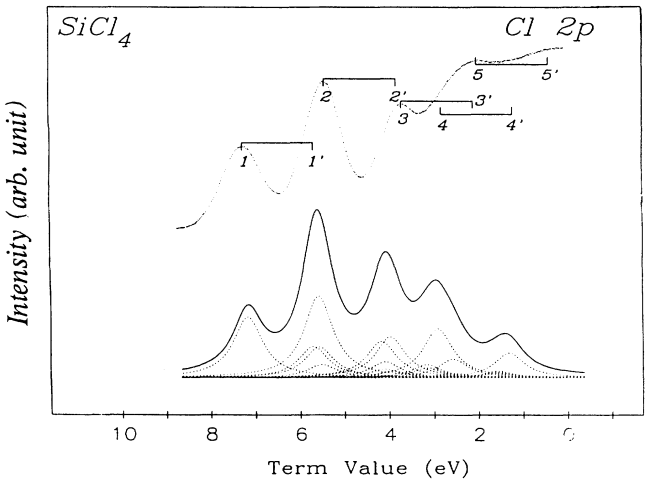

FIG. 4. Experimental (top) and simulated (bottom, shifted by 0.7 eV, see text) Cl 2*p* photoabsorption spectra of $SiCl_4$.

TABLE III. Experimental and calculated Cl $2p$ pre-edge structures for $SiCl_4$.

Line	Experiment (eV)	Experimental term value (eV)	Calculated term value (eV)	Oscillator strength	Assignment
1	201.68	5.22	5.97	3.94×10^{-3}	$16a_1^*$
1′	203.28				
2	203.54	3.36	4.50	2.01×10^{-3}	$17a_1^*$
2′	205.14		4.38	5.27×10^{-3}	$13e^*$
			4.31	8.28×10^{-4}	$18a_1^*$
3	205.26	1.64	2.98	2.35×10^{-3}	$19a_1^*$
3′	206.86		2.92	6.18×10^{-4}	$14e^*$
4	206.15	0.75	1.97	8.22×10^{-4}	$20a_1^*$
4′	207.75		1.95	3.16×10^{-3}	$15e^*$
5	206.94	−0.04	1.72	5.40×10^{-4}	$16e^*$
5′	208.54				

Again this splitting is due to the splitting of the T_d $10t_2^*$ orbital into its C_{3v} e^* and a_1^* components.

The experimental Cl $2p$ photoabsorption spectrum presented on a term value scale is shown in the top curve of Fig. 4, where a weighted average of the spin-orbit components was used as the Cl $2p$ ionization potential. The Cl ionization edges are difficult to locate precisely from the spectrum. From x-ray photoelectron spectroscopy, the energy of the Cl $2p_{3/2}$ photoelectron peak in $SiCl_4$ was observed at 206.9 eV.[45] Using a Cl $2p_{3/2}$−Cl $2p_{1/2}$ spin-orbit splitting of 1.6 eV,[45] five absorption bands (labeled 1–5) can be identified from the spectrum. Positions of the assorted peaks in the photoabsorption spectrum are tabulated in Table III.

The electron charge distribution of the unoccupied orbitals obtained from the localized Cl $2p$ core-hole transition-state potential are presented in Table IV. The character of the empty orbitals and their energy ordering in the Cl $2p$ hole state are very similar to the corresponding orbitals in the Si core-hole states. As mentioned previously, in the localized Cl core-hole approximation, orbitals of t_2 symmetry are split into a_1 and e. The Si—Cl antibonding $17a_1^*$ and $13e^*$ orbital can be correlated with the antibonding $9t_2^*$ orbital in the T_d molecule. Similarly, the Rydberg $9a_1^* + 14e^*$ and $10a_1^* + 15e^*$ orbitals can be compared with the $10t_2^*$ and $11t_2^*$ orbitals, respectively. The calculated total oscillator strengths from the a_1 and e orbitals of Cl $2p$ to the unoccupied orbitals are compared with the experimental absorption features in Table III. The transitions to the Si—Cl antibonding $16a_1^*$, $17a_1^*$, and $13e^*$ orbitals are predicted to be strong. The theoretical results also show that the transitions to the Rydberg p ($9a_1^*$) and Rydberg p and d ($8e^*$) orbitals will contribute significantly to the absorption spectrum. A stimulated Cl $2p$ photoabsorption spectrum employing the theoretical transition energies and oscillator strengths collected in Table III, assuming a Cl $2p$ spin-orbit splitting of 1.6 eV and then convoluted with Lorentzian line shapes of linewidth 0.8 eV to mimic the instrumental resolution is shown in the bottom curves of Fig. 4. The agreement between the theoretical and experimental spectra is good if the peaks are shifted by ~0.7 eV. The first two intense peaks (1,1′ and 2,2′) in the experimental spectrum can be readily assigned to the transitions into the antibonding $16a_1^*$, $17a_1^*$, and $13e^*$ orbitals. According to the calculations, transitions to the higher Rydberg orbitals are responsible for the absorption features 3–5. These assignments for the Cl $2p$ photoabsorption spectrum are consistent with those proposed for the Si core-level (*vida infra*).

TABLE IV. Orbital charge distribution for the unoccupied orbitals in the Cl $2p$ core transition state of $SiCl_4$.

Orbital	Q_{out}	Q_{int}	Q_{Si}	Q_{Cl^*}	Q_{Cl}	Remarks
$16a_1^*$	0.07	0.11	0.27	0.16	0.59	Si—Cl antibonding
$17a_1^*$	0.12	0.40	0.25	0.06	0.17	Si—Cl antibonding
$13e^*$	0.06	0.39	0.27	0.06	0.21	Si—Cl antibonding
$18a_1^*$	0.37	0.46	0.06	0.01	0.01	Rydberg s
$19a_1^*$	0.52	0.34	0.06	0.04	0.05	Rydberg p
$14e^*$	0.52	0.32	0.08	0.01	0.07	Rydberg p
$20a_1^*$	0.66	0.29	0.01	0.01	0.03	Rydberg p and d
$15e^*$	0.65	0.29	0.01	0.02	0.03	Rydberg p and d
$16e^*$	0.77	0.18	0.00	0.01	0.04	Rydberg d
$21a_1^*$	0.94	0.05	0.00	0.00	0.01	Rydberg s

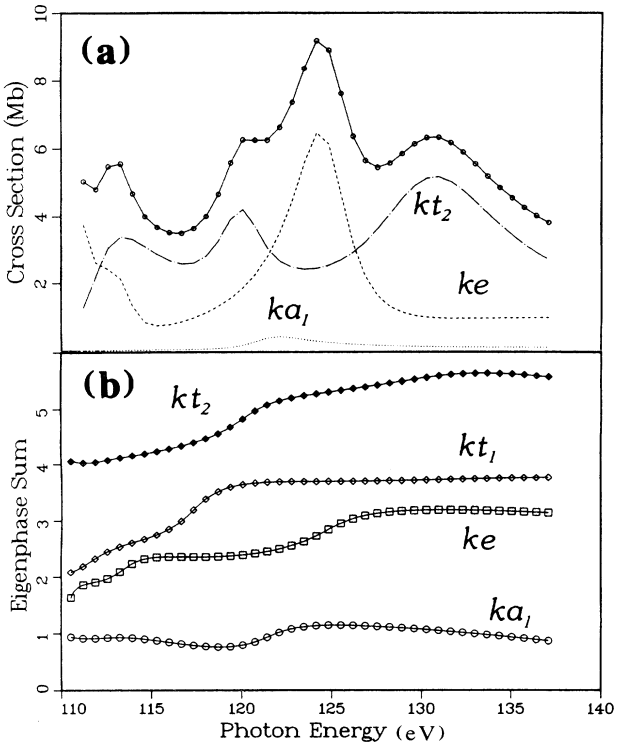

FIG. 5. Si $2p$ (a) photoionization cross section, and (b) Eigenphase sum for continuum channels of $SiCl_4$.

The post-edge NEXAFS region

Although a previous paper[4] has used the published Si $2p$ MS $X\alpha$ calculations[18] to interpret the above-edge spectra of the Si $2p$ and Si $2s$ edges, we report here our MS $X\alpha$ calculations for all three Si edges because they provide additional insight.

Our cross-section results for the Si $2p$ spectrum [Fig. 5(a)] are identical to the previous calculations, and the gross features are in reasonable agreement with experiment (Table V). The calculations predict six resonances in the energy range from threshold to 30 eV beyond the ionization potential. The principal contribution close to the threshold are two weak resonances in the kt_2 and ke continuum channels. At 14 eV, the resonance in the ke channel dominates the cross section; the kt_2 cross section maximizes at about 20 eV above threshold. The ka_1 continuum channel has a very small contribution at 12 eV beyond threshold and excitation through the kt_1 channel has negligible cross section.

TABLE V. Experimental and calculated near-edge structures for $SiCl_4$.

Level	Experimental term value (eV)	Calculated term value (eV)	Assignment
Si $2p$	−1.3	−2.7	ke, kt_2
	−4.9		
	−7.0	−10.0	kt_2
	−9.4	−12.0	ka_1
	−11.8	−14.0	ke
	−22.5	−20.0	kt_2
Si $2s$	−0.8	−1.0	kt_2
	−7.4	−6.8	kt_2
		−10.2	kt_2
	−12.6		ke?
	−19.3	−20.1	kt_2
Si $1s$	−0.3	−0.7	kt_2
	−7.0	−6.8	kt_2
		−10.2	kt_2
	−9.8		ke?
	−24.1	−20.4	kt_2

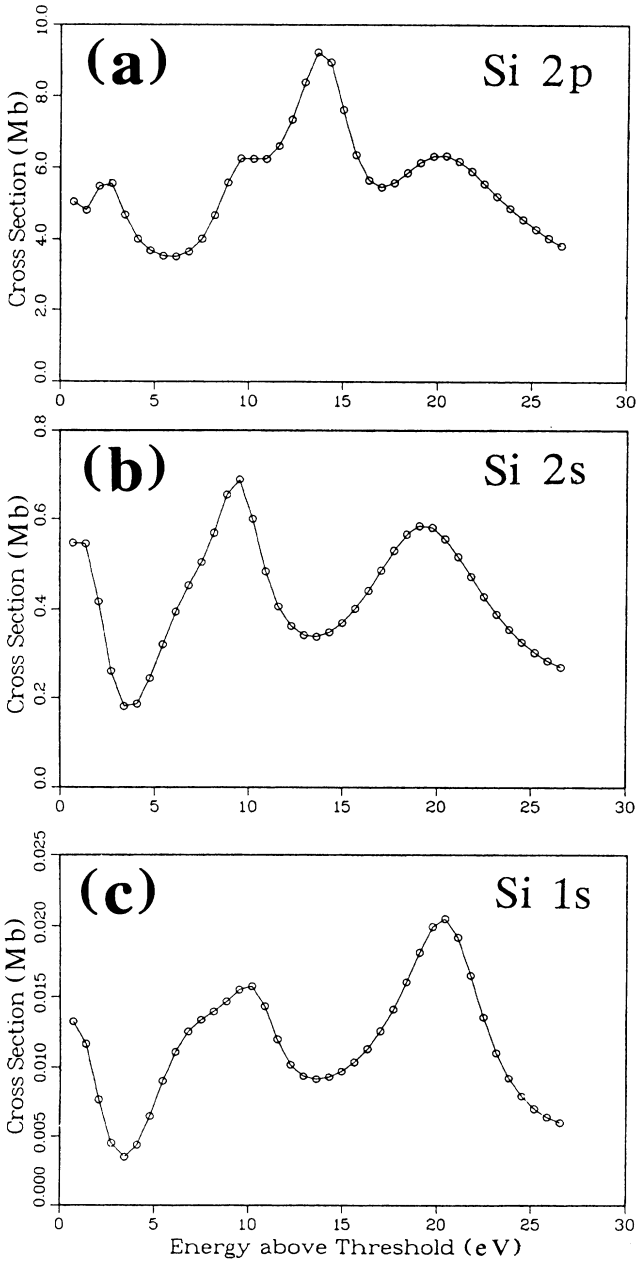

FIG. 6. Photoionization cross sections for (a) Si $2p$, (b) Si $2s$, and (c) Si $1s$ orbital of $SiCl_4$.

The eigenphase sum analysis has not been previously reported, and is worth commenting on here to better characterize the resonances. The eigenphase sum is a characteristic of the exit channel in the photoionization process.[46] For a noninteracting photoelectron, the continuum wave function is a plane wave and the eigenphase sum is a smooth function of the kinetic energy. Scattering of the photoelectron by the molecular potential will produce a phase shift and change the eigenphase sum.[47] Resonances in the continuum channel are normally associated with a rapid change in the eigenphase sum over a small energy interval.[48] To demonstrate this effect, we displayed the eigenphase sum for the dipole allowed exit continuum channels for the Si $2p$ ionization as a function of energy in Fig. 5(b). As anticipated, the increase in cross section in the ke channel at 14 eV is accompanied by a rapid change of the phase shift. Similarly, the resonances at 12 eV for the ka_1 channel and at 7 eV for the kt_2 channel are signified by a rapid change in the phase of the respective eigenchannel. However, the kt_2 cross-section maxima calculated at 2.7 and 20 eV beyond threshold are not reflected in the eigenphase sum. These two resonances are most likely due to the diffraction of photoelectron by the surrounding ligands,[16,49,50] rather than *shape* resonances.

The theoretical Si $2s$ and Si $1s$ spectra are shown in Fig. 6, along with the theoretical Si $2p$ spectrum. Since kt_2 is the only symmetry-allowed exit channel for an s orbital excitation, the calculated s cross sections correspond to the partial kt_2 continuum channel in the Si $2p$ cross section [Fig. 5(a)]. As expected, the Si $2s$ and Si $1s$ cross sections are very similar, and there is reasonable agreement with experiment in both cases. The theoretical cross-section maxima with term values of -1, -10, and -20 eV are correlated with the experimental features[4] at approximately -0.5, -7, and -20 eV. The experimental spectra show hints of peaks between -10 and -12 eV which have been assigned to symmetry-forbidden ke excitations.[4] The theoretical peaks at ~ -10 eV show very distinct shoulders at ~ -7 eV. Close examination of the corresponding Si $2s$ and Si $1s$ experimental peaks shows that they are distinctly asymmetric, in accord with theory. As with high-energy Si $2p$ peak, at ~ -20 eV, the high-energy Si $2s$ and Si $1s$ resonances do not show appreciable eigenphase sum changes, and these resonances are most likely due to photoelectron diffraction.

CONCLUSIONS

The Si $1s$, $2s$, $2p$ and Cl $1s$ and $2p$ core-level photoabsorption spectra have been assigned with the aid of MS $X\alpha$ calculations. The pre-edge and near-edge structures in the s-level spectra can be readily assigned to transitions into final states of t_2 symmetry, and there is semiquantitative agreement between theory and experiment for both positions and relative intensities. In the pre-edge region, the strong peak originates from the transition to the Si—Cl antibonding and $9t_2^*$ orbital, while the broader, weaker peak near threshold is due to transitions to Rydberg orbitals.

The complex Si $2p$ pre-edge spectrum cannot be unambiguously assigned with our calculations. The two strongest pre-edge absorptions are assigned to Si $2p \rightarrow 8a_1^*$ and $2p \rightarrow 9t_2^*$ transitions, but the calculated intensities for the Rydberg transitions are much too small, and the intensities of the bands originating from the Si $2p_{1/2}$ level are stronger than those from the Si $2p_{3/2}$. More elaborate theoretical calculations are now needed to settle these problems. There is good agreement between the theoretical and experimental Si $2p$ NEXAFS spectrum, but our eigenphase sum results show that the high-energy resonances (~ 20 eV above the edge) in all Si spectra are probably due to photoelectron diffraction and are not true *shape* resonances.

MS $X\alpha$ calculations based on a localized Cl core-hole approximation gave a satisfactory description of the Cl $2p$ photoabsorption spectrum. The assignment of the Cl $2p$ spectrum is very similar to that of the Si $2p$. Excitations to the antibonding orbitals are shown to be responsible for the intense peaks at low energies. The Cl $2p \rightarrow$ Rydberg transitions can be correlated with the features at higher energies. It is perhaps surprising to note that, unlike the Si $2p$ spectrum, there is reasonable agreement between the theoretical and experimental intensities.

*To whom correspondence should be addressed.

[1] C. E. Brion, D. David, R. Sodhi, and A. P. Hitchcock, in *X-ray and Atomic Inner Shell Physics,* Proceedings of the International Conference on X-ray and Atomic Inner Shell Physics, University of Oregon, 1982, AIP Conf. Proc. No. 94, edited by B. Crasemann (AIP, New York, 1982), pp. 429-446.

[2] G. Margaritondo, *Introduction to Synchrotron Radiation* (Oxford University Press, New York, 1988).

[3] A bibliography of inner-shell spectra of molecules is given by A. P. Hitchcock, J. Electron. Spectrosc. **25**, 245 (1982).

[4] J. D. Bozek, K. H. Tan. G. M. Bancroft, and J. S. Tse, Chem. Phys. Lett. **138**, 33 (1987).

[5] E. Ishiguro, S. Iwata, A. Mikuni, Y. Suzuki, H. Kanamori, and T. Sasaki, J. Phys. B **20**, 4725 (1987).

[6] K. H. Sze, C. E. Brion, X. M. Tong, and J. M. Li, Chem. Phys. **115**, 433 (1987).

[7] J. Dehmer, J. Chem. Phys. **56**, 4496 (1972).

[8] M. B. Robin, Chem. Phys. Lett. **119**, 33 (1985).

[9] J. Dehmer, A. C. Parr, and S. H. Southworth, *Resonances in Molecular Photoionization,* in Vol. II of *Handbook of Synchrotron Radiation,* edited by G. V. Mar (North-Holland, Amsterdam, 1986); M. B. Robin, *Higher Excited States of Polyatomic Molecules* (Academic, New York, 1985), Vol. IV.

[10] V. I. Nefedov, J. Struct. Chem. **9**, 217 (1968).

[11] P. W. Langhoff, American Chemical Society Symposium Series No. 263, Resonances in Electron and Molecular Scattering, van der Waals Complexes and Reactive Dynamics, edited by D. G. Truhlar (American Chemical Society, Washington, D.C., 1984), p. 113.

[12] F. Keller and H. Lefebvre-Brion, Z. Phys. D **4**, 15 (1986).

[13]J. E. Bice, K. H. Tan, G. M. Bancroft, and J. S. Tse, J. Chem. Phys. **87**, 621 (1987).
[14]J. E. Bice, K. H. Tan, G. M. Bancroft, and J. S. Tse, Inorg. Chem. **26**, 4106 (1987).
[15]B. W. Yates, G. M. Bancroft, L. L. Coatsworth, J. S. Tse, and G. Schrobilgen, J. Chem. Phys. **84**, 3603 (1986).
[16]J. S. Tse, J. Chem. Phys. **89**, 920 (1988).
[17]S. Bodeur, I. Nenner, and P. Millie, Phys. Rev. A **34**, 2986 (1986).
[18]T. A. Carlson, N. A. Svensson, M. O. Krause, T. A. Whitley, F. A. Grimm, G. von Wald, J. W. Taylor, and B. P. Pullen, J. Chem. Phys. **84**, 122 (1986).
[19]T. M. Zimkina and A. S. Vinogradov, J. Phys. (Paris) Colloq. **32**, C4-3 (1971).
[20]V. F. Fomichev, T. M. Zimkina, A. S. Vinogradov, and A. M. Evdokimov, J. Struct. Chem. **11**, 626 (1970).
[21]K. H. Johnson, Adv. Chem. Phys. **7**, 143 (1973).
[22]J. C. Slater, *The Calculation of Molecular Orbitals* (Wiley-Interscience, New York, 1979).
[23]L. Noodleman, J. Chem. Phys. **64**, 2343 (1976).
[24]J. Dehmer and D. Dill, Phys. Rev. Lett. **35**, 213 (1975).
[25]J. W. Davenport, Phys. Rev. Lett. **36**, 945 (1976).
[26]R. Roberge and D. R. Salahub, J. Chem. Phys. **70**, 1177 (1979).
[27]J. S. Tse, D. J. Bristow, G. M. Bancroft, and G. Schrobilgen, Inorg. Chem. **18**, 1766 (1979).
[28]D. K. Creber, J. S. Tse, and G. M. Bancroft, J. Chem. Phys. **72**, 4291 (1980).
[29]J. Dehmer and D. Dill, *Electron-Molecule and Photon-Molecule Collisions,* edited by T. Rescigno, V. McKoy, and B. Schneider (Plenum, New York, 1979).
[30]J. C. Slater, *The Self-consistent Field for Molecules and Solids* (McGraw-Hill, New York, 1974), Vol. IV.
[31]J. Dehmer, Ref. 11, p. 139.
[32]T. A. Carlson, A. Fahlman, M. O. Krause, T. A. Whitley, F. A. Grimm, M. N. Piancastelli, and J. W. Taylor, J. Chem. Phys. **84**, 641 (1986).
[33]L. Latter, Phys. Rev. **99**, 510 (1955).
[34]J. S. Tse, D. K. Creber, and G. M. Bancroft, J. Chem. Phys. **74**, 3097 (1981).
[35]L. C. Synder, J. Chem. Phys. **55**, 95 (1971).
[36]L. S. Cederbaum and W. Domcke, J. Chem. Phys. **66**, 5084 (1977).
[37]H. Friedrich, B. Pittel, P. Rabe, W. H. E. Schwarz, and B. Sonntag, J. Phys. B **13**, 25 (1980).
[38]R. S. Mulliken, Acc. Chem. Res. **9**, 7 (1976).
[39]E. Lindholm, Ark. Fys. **40**, 97 (1969).
[40]M. B. Robin, *Higher-Excited States of Polyatomic Molecules* (Academic, New York, 1974), Vol. I.
[41]H. A. Jahn and E. Tell, Proc. R. Soc. London, Ser. A **161**, 220 (1937).
[42]J. W. Rabalais, *Principle of Ultraviolet Photoelectron Spectroscopy* (Wiley, New York, 1977).
[43]A. P. Hitchcock, G. R. J. Williams, C. E. Brion, and P. W. Langhoff, Chem. Phys. **86**, 65 (1984).
[44]S. Bodeur, J. C. Ferrer, I. Nenner, P. Millie, M. Benfatto, and C. R. Natoli, J. Phys. (Paris) Colloq. **48**, C9-1117 (1987).
[45]J. E. Drake, C. Riddle, and L. Coatsworth, Can. J. Chem. **53**, 3602 (1975).
[46]J. Macek, Phys. Rev. A **3**, 1101 (1970).
[47]L. I. Schiff, *Quantum Mechanics* (McGraw-Hill, New York, 1955).
[48]J. Kreile, A. Schweig, and W. Thiel, Chem. Phys. Lett. **105**, 259 (1984).
[49]T. Fujikawa, J. Phys. Soc. Jpn. **50**, 1321 (1981).
[50]A. Bianconi, *X-ray Absorption: Principles, Applications, Techniques of EXAFS, SEXAFS and XANES,* edited by D. C. Koningsberger and R. Prins (Wiley, New York, 1988).